Pre-normative REsearch for Safe use of Liquid Hydrogen (PRESLHY)

Project Deliverable

Theory and Analysis of Cryogenic Hydrogen Release and Dispersion

Deliverable Number:	18 (D3.1)
Version	1.1
Author(s):	Alexandros Venetsanos NCSRD
Submitted Date:	4 August 2019
Due Date:	30 June 2019
Report Classification:	Public

FUEL CELLS AND HYDROGEN
JOINT UNDERTAKING

This project has received funding from the Fuel Cells and Hydrogen 2 Joint Undertaking under the European Union's Horizon 2020 research and innovation programme under grant agreement No 779613.

History		
Nr.	Date	Changes/Author
1.0	4.8.2019	Submitted reviewed version
1.1	15.1.2020	Corrected cover page

Approvals / Revisions			
	Name	Organisation	Date
Coordinator	Thomas Jordan	KIT	6.8.2019
Partner	Frank Markert	HYSAFE	
Partner	Jennifer Wen	UWAR	
WP leader	Simon Coldrick	HSL	
	Thomas Jordan	KIT	Front page updated

Acknowledgments

This project has received funding from the Fuel Cells and Hydrogen 2 Joint Undertaking under the European Union's Horizon 2020 research and innovation programme under grant agreement No 779613.

Disclaimer

Key words

release, dispersion, liquid hydrogen, cryogenic hydrogen, multiphase, multicomponent

Terminology

Cryogenic	Refers to temperatures below 100 K
Evaporation	Change from liquid to vapour below boiling temperature
Vaporization	Change from liquid to vapour at boiling temperature
Condensation	Change from vapour to liquid
Sublimation	Change from solid to vapour
Deposition	Change from vapour to solid
Freezing	Change from liquid to solid
Melting	Change from solid to liquid

Table of Contents

0 Nomenclature

Latin symbol	Physical meaning	Units
A	Cross sectional area	m^2
D	Hydraulic diameter	m
f	Darcy friction coefficient	-
U	Velocity	m/s
h	Enthalpy	J/kg
v	Specific volume	m^3/kg
J	Diffusive mass flux	$kg/m^2/s$
P	Pressure	Pa
s	Entropy	J/kg/K
T	Temperature	K
Y	mass fraction in mixture	-
y	Mass fraction of the total stable phase (vapour + liquid)	-
t	time	s
M	Molecular weight	kg/kmol
k	Turbulent kinetic energy	m^2/s^2
q	Heat flux	$J/m^2/s$
c_P	Specific heat under constant pressure	J/kg/K

Greek symbol	Physical meaning	Units
α	Void fraction	-
Γ	Phase change mass flux	kg/s
θ	Thermal relaxation time of HRM model	s
μ	Dynamic viscosity	Pa s
ρ	Density	kg/m^3
λ	Thermal conductivity	W/m/K
τ	Shear stress tensor	Pa

Subscript	Physical meaning
0	Stagnation conditions
1	Upstream location
2	Downstream location
b	Back pressure
con	Condensation
vap	Vaporization
CR	Critical thermodynamic point
LM	Liquid in metastable condition
LS	Liquid saturated
onset	Nucleation onset
VS	Vapour saturated
Sat	Saturated conditions
HEM	Homogeneous Equilibrium model
L	Non-vapour state (liquid or solid)
V	Vapour state
k	Mixture component
S	Slip
D	Drift

1 Introduction

The objective of this contribution is to perform a critical review of the modelling work on cryogenic hydrogen release and dispersion. The various modelling approaches are examined with the aim to clarify our level of understanding of the various phenomena involved, identify their differences, their weaknesses and strengths, and finally draw conclusions regarding our current modelling abilities and needs for further research.

The word “cryogenic” in general refers to temperatures below 100 K, so when cryogenic hydrogen release and dispersion is investigated, hydrogen can be in vapour state, liquid state, two-phase (liquid-vapour) state or supercritical state.

Cryogenic conditions for hydrogen dispersion in air apply to a region close enough to the cold source (near field) were temperatures are low enough to condense main components, oxygen and nitrogen, of the ambient air. Further away from the source (far field), temperatures are increased mainly due to heating from ground and ambient atmosphere and the hydrogen-air cloud will be a fully gaseous non-cryogenic, multicomponent mixture. Modelling of the far field of course requires knowledge of the near field conditions and therefore modelling of the cryogenic near field is required.

In the simplest case of cryogenic gaseous hydrogen dispersion in air, air humidity in the near field will condense and freeze and possibly, depending on the temperature, oxygen and nitrogen of the ambient air will condense and freeze too. If two-phase hydrogen exists at the source (approximately 20 K saturation temperature at 1 atm ambient pressure) then the physical problem in the near field gets more complicated. In both cases, the resulting hydrogen-air near field cloud will be a multiphase, multicomponent mixture.

Modelling of multiphase, multicomponent mixture flow and dispersion poses far greater challenges than that of single-phase and single-component flows. These challenges are due to interfaces between phases and large or discontinuous property variations across interfaces between phases and/or components.

Two approaches are commonly used for the simulation of multiphase and multicomponent flows, a) the homogeneous mixture approach and b) the distinct volume approach, see Lagumbay et al. (2007).

In the first approach, the phases and/or components are spatially averaged to lead to a homogeneous mixture and are considered to occupy the same volume. This homogeneous mixture can either be in equilibrium (e.g., the mechanical and thermal properties are in equilibrium) or in non-equilibrium (e.g., the mechanical and/or thermal properties are not in equilibrium) conditions.

In the second approach, each phase and/or component is considered to occupy a distinct volume and the interfaces between the phases and/or components are tracked explicitly. This approach is often also referred to as the volume of fluid (VOF) method.

In this work main focus is given to the homogeneous mixture approach, since as will be shown, this approach has been extensively used in simulations of cryogenic hydrogen dispersion in ambient air.

The document is organized as follows. The first chapter examines cryogenic hydrogen physical properties and their modelling and differences between cryogenic hydrogen, cryogenic helium and cryogenic natural gas are outlined.

The second chapter presents in detail the CFD modelling of multiphase, multicomponent hydrogen flow and dispersion in air using the homogeneous mixture approach. Differences between various modelling approaches regarding cryogenic hydrogen flow and dispersion are reviewed and outlined.

Integral modelling approaches are examined in the third chapter. The wording “integral” here refers to models in which 3d conservation equations are essentially integrated / averaged over some hydrogen containing space to produce 0d, 1d or 2d equations. Such integral modelling approaches

include 0d release modelling, 0d notional-nozzle modelling, 1d jet-plume modelling and 2d shallow layer cryogenic pool modelling.

The fourth chapter examines similarity laws derived from theoretical arguments and experiments with focus on cryogenic momentum dominated hydrogen jets and their comparison against their non-cryogenic counterparts.

In the final chapter, conclusions are drawn and suggestions for future work are given.

2 Physical properties

2.1 Hydrogen

Hydrogen thermo-physical physical properties can be obtained using various Equation of State (EoS) formulations. The level of complexity of the EoS formulation to be used in a given simulation depends on the application and more specifically on the thermodynamic conditions encountered during the simulation of the given application.

The most accurate, but also the most computationally expensive modern EoS formulation covering in a continuous way the entire range of liquid, supercritical and vapour states was presented by Leachman et al. (2009), see also (NIST, 2019). It is based on explicit modelling of the Helmholtz Free Energy in terms of density and temperature and contains a large set of coefficients. Within this formulation thermo-physical properties are calculated using partial derivatives of the free energy.

Leachman's NIST formulation has been either directly implemented in various simulation codes, e.g. Travis et al. (2013), Venetsanos and Giannissi (2017) or linked to the NIST REFPROP software Lemmon et al. (2013), e.g. Jin et al. (2017) and Houf and Winters (2013).

EoS formulations, simpler than Leachman's NIST, but covering in a continuous way the entire range of thermodynamic states (except solid) have been reviewed by Nasrifar (2010). Eleven cubic equations of state were examined and compared against experimental data and the modified Redlich–Kwong EoS by Mathias and Copeman (1983) was found to be the most accurate and robust.

The Abel Noble EoS formulation widely used in non-cryogenic hydrogen simulations was compared to that of NIST EoS for cryogenic gaseous conditions by Cirrone et al., (2019b). The study showed that Abel-Noble EoS can be applied to gaseous releases at cryogenic temperatures for pressure up to 6 bara, given that a negligible difference was observed between the density calculated using the two EoSs, as shown in Figure 1.

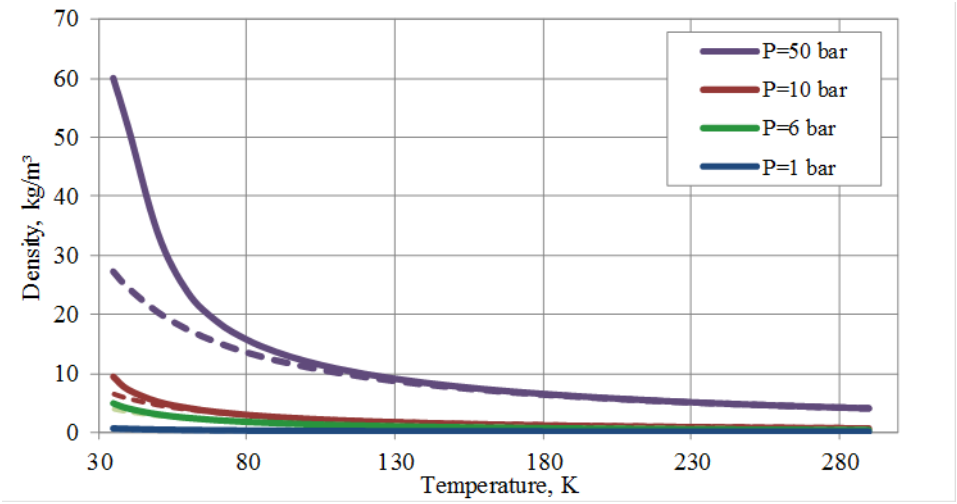

Figure 1 Effect of EOS on density evaluation: NIST (—) versus Abel Noble (--) equations.

When the pressure in a given two-phase hydrogen dispersion scenario is practically atmospheric (i.e. nearly 1 atm), simulations are often performed using ideal gas relations for hydrogen vapour and correlations for hydrogen liquid, taken e.g. from Poling et al (2004), where a correlation for the specific enthalpy of vaporization needs also to be provided to bridge the liquid and vapour conditions. The ideal gas approximation is generally a valid approach for low pressures and can be safely applied for atmospheric pressure conditions.

It is known that hydrogen vapour specific heat at given pressure (or density) starts to increase when temperature is reduced below a given limit, see Markert et al. (2014). Figure 2 below shows real hydrogen vapour specific heat as function of temperature for atmospheric and for zero pressure

(ideal gas theoretical limit). At 20.37 K (saturation temperature at 1 atm) the deviation from the ideal gas is 16.7%. The larger specific heat implies that lower temperatures and consequently lower densities will persist longer close to a two phase source during dispersion.

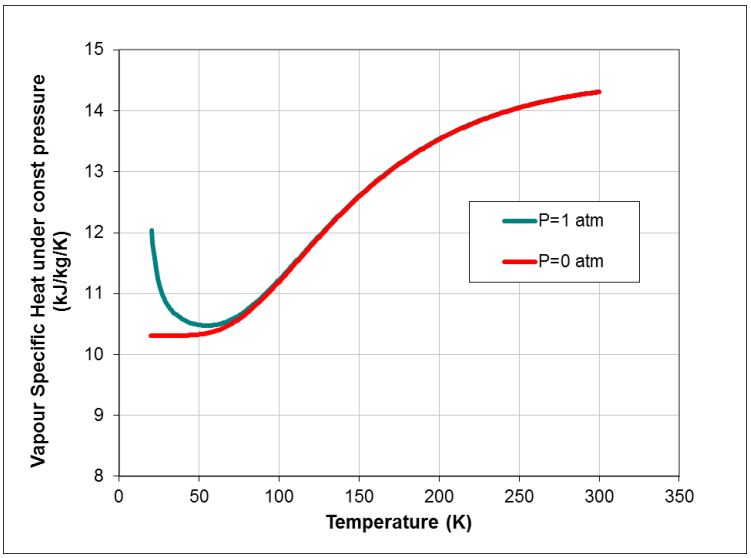

Figure 2 Hydrogen vapour specific heat at two pressures (values from NIST chemistry web-book)

2.2 Comparison with other cryogenic substances

Liquid helium has been used in the past in dispersion experiments as a surrogate of liquid hydrogen due to safety reasons, see Proust et al. (2001).

As reported by Venetsanos et al. (2019), similar to hydrogen, helium vapour specific heat gradually increases at 1 bar as saturation temperature (4.23 K) is approached: 9082.7, 5250.8 and 5193.1 J/kg/K at 4.23, 20 and 30 K respectively. The higher vapour specific heat implies lower temperatures, lower densities and therefore more pronounced dense gas behaviour.

When comparing cryogenic hydrogen to cryogenic helium special attention should also be given to their pronounced difference regarding enthalpy of vaporization. At 1 bar, enthalpy of vaporization of helium is approximately 23 times lower than that of hydrogen (with values 20.7 and 473.4 kJ/kg respectively). This implies that liquid helium will turn into vapour much faster than hydrogen.

Comparison of safety-related physical properties of liquid hydrogen and liquid natural gas has been performed by Klebanoff et al. (2017).

A comparative CFD assessment study of cryogenic hydrogen and LNG dispersion has been performed by Giannissi and Venetsanos (2019).

An important difference between liquid hydrogen and liquid natural gas dispersion in ambient air exists that makes modelling of liquid hydrogen dispersion much more complex. In the case of liquid hydrogen dispersion oxygen and nitrogen of the ambient air will become liquid or even solid close to the release, since their freezing temperatures (54.4 K and 63.3 K respectively) and boiling temperatures (90.2 and 77.4 K respectively) are much higher than the hydrogen boiling temperature (20.4 K). In the case of liquid natural gas having a boiling point of 111.7 K (for methane), cryogenic conditions are not reached, i.e. oxygen and nitrogen will always remain in gaseous state.

3 CFD modelling of two-phase multicomponent hydrogen flow and dispersion in air using the homogeneous mixture approach

3.1 Review of previous simulation studies

Previous state of the art and knowledge gaps reviews were performed by Ekoto et al. (2014) and Dolci et al. (2018). In the present review focus is given to simulation studies / strategies. These are categorized in Table 1 below by experiment modelled.

Test-6 of the NASA large scale liquid hydrogen spill experiments on flat ground, see Witcofski and Chirivella (1984), involving a spill of 5.11 m^3 of liquid hydrogen in 38 s (average flow rate of 9.5 kg/s) was simulated by Venetsanos and Bartzis (2007), Middha et al. (2011), Liu et al. (2018), Sklavounos and Rigas (2005) as well as Molkov et al. (2005). Different approaches regarding source modelling as well as phase change modelling have been used in these studies.

Test-5 of the BAM large-scale liquid hydrogen spill tests adjacent to buildings, see Marinescu-Pasoi and Sturm (1994) and Verfondern and Dienhart (1997), was simulated by Statharas et al. (2000) using the ADREA-HF code using a release rate of 0.37 kg/s for a period of 125 s.

Test-3 of the INERIS large scale liquid helium release experiments on flat ground, see Proust et al. (2001), was very recently simulated by Venetsanos et al. (2019), using the ADREA-HF code. Liquid helium was used in the experiments as a surrogate for liquid hydrogen for safety reasons.

The HSL/HSE large scale two-phase hydrogen jet release experiments, see Hooker et al. (2011), consisted of four tests with different release directions and duration and a constant release rate of 60 L/min from a 2.63 cm nozzle. Test 5 was a horizontal release 3.4 mm from ground, tests 6 was a vertical release downwards from 10 cm height and test 7 a horizontal release at 86 cm from ground.

Tests 6 and 7 were simulated by Ichard et al. (2012) using FLACS code. Uncertainty in the hydrogen vapour quality at the nozzle exit led the authors to perform a related sensitivity study, which showed that results were highly affected by the exit vapour quality value assumed.

Tests 5, 6 and 7 were simulated by Giannissi et al. (2014) using ADREA-HF code with main focus to study the effect of humidity as well as the effect of fluctuating ambient wind velocity. Equilibrium (HEM) and non-equilibrium approaches (HNEM) were applied. In the second case only mechanical non-equilibrium was assumed and an algebraic slip model was used to account for slip of hydrogen and water droplets.

Giannissi and Venetsanos (2018) simulated test 7 giving focus on the condensation of both humidity and ambient air components (nitrogen and oxygen) and application of a HNEM approach using momentum conservation equations for the liquid phase instead of the algebraic approach used earlier. Nozzle exit conditions in these studies were calculated assuming isenthalpic expansion from reported stagnation conditions in the storage tank (2 bars).

Selected KIT experiments from Veser et al. (2011) and Friedrich et al. (2012) concerning under-expanded cryogenic hydrogen jets emerging from cryo-compressed hydrogen storage, were simulated by Venetsanos and Giannissi (2017) using the ADREA-HF code.

A comparative CFD assessment study of cryogenic hydrogen and LNG dispersion was performed by Giannissi and Venetsanos (2019).

In all works referenced above the homogeneous mixture approach has been used in the CFD simulations of two-phase hydrogen dispersion in ambient air. The homogeneous mixture approach is presented in detail in the following sections.

Table 1: Cryogenic hydrogen experiments and respective CFD simulations

Experiment	Reference	Description	CFD studies
NASA-6	Witcofski and Chirivella (1984)	Liquid hydrogen on flat ground, 11.5 kg/s for 38 s	Sklavounos and Rigas (2005), Molkov et al. (2005), Venetsanos and Bartzis (2007), Middha et al. (2011), Liu et al. (2018)
BAM-5	Marinescu-Pasoi and Sturm (1994) and Verfondern and Dienhart (1997)	Liquid hydrogen between buildings, 0.4 kg/s for 700 s	Statharas et al. (2000)
INERIS-3	Proust et al. (2001)	Liquid helium on flat ground, 2.12 kg/s for 52 s	Venetsanos et al. (2019)
HSL	Hooker et al. (2011)	Liquid hydrogen on flat ground and horizontally above ground, 0.07 kg/s for 305 s	Ichard et al. (2012), Giannissi et al. (2014), Giannissi and Venetsanos (2018)
KIT	Veser et al. (2011)	Steady under-expanded hydrogen jets, Stagnation: P = 5-60 bar, T = 35 and 80 K, nozzle diameters 1, 2 and 4 mm	Venetsanos and Giannissi (2017)
KIT	Friedrich et al. (2012)	Steady under-expanded hydrogen jets, Stagnation: P = 7-35 bar, T = 35-65 K, nozzle diameters 0.5 and 1 mm	Venetsanos and Giannissi (2017)
SNL	Hecht and Panda (2018)	Steady under-expanded hydrogen jets, Stagnation: P = 2-5 bar, T = 48-63 K, nozzle diameters 1 and 1.25 mm	Giannissi et al. (2019)

3.2 Mixture definition and physical properties

In the homogeneous mixture approach for cryogenic hydrogen dispersing into ambient air the working fluid is assumed to be a multi-component two-phase ideal mixture, in which non-vapour phase (liquid or solid) is dispersed homogeneously into the prevailing vapour phase.

The usual way of describing the mixture components is through their mass fractions in the mixture. By definition, the sum of the component total mass fractions always equals to one, where the total mass fraction for a given component is the sum of the vapour and the non-vapour mass fractions.

$$1 = \sum_k Y_k = \sum_k \left(Y_{Vk} + Y_{Lk} \right) \tag{1}$$

Alternatively, instead of mass fractions, mixture fractions have also been used, but in the present work mass fractions will be used. Mixture fractions are related to mass fractions through the relation below, where subscript “0” denotes initial conditions (time zero), “air” denotes in ambient air and “src” denotes at source.

$$f_{Vk} = \frac{Y_{Vk} - Y_{Vk0}^{air}}{Y_{Vk0}^{src} - Y_{Vk0}^{air}}, \quad f_{Lk} = \frac{Y_{Lk} - Y_{Lk0}^{air}}{Y_{Lk0}^{src} - Y_{Lk0}^{air}} \tag{2}$$

For ideal mixtures, mixture physical properties are calculated using phase-component physical properties, through simple linear dependencies on the component mass fraction. In non-ideal mixtures such dependencies may not be linear. Phase-component physical properties are generally assumed to be functions of mixture pressure and temperature.

Mixture density:

$$\frac{1}{\rho} = \sum_k \frac{Y_k}{\rho_k} = \sum_k \left(\frac{Y_{Vk}}{\rho_{Vk}} + \frac{Y_{Lk}}{\rho_{Lk}} \right) \tag{3}$$

The mixture density equation states that the mixture volume is the sum of the volumes occupied by the mixture components.

Volume fraction is often used in two-phase analysis and is defined as follows:

$$\alpha_{Vk} = \frac{\rho Y_{Vk}}{\rho_{Vk}}, \quad \alpha_{Lk} = \frac{\rho Y_{Lk}}{\rho_{Lk}} \tag{4}$$

The following identity holds:

$$1 = \sum_k \alpha_k = \sum_k \left(\alpha_{Vk} + \alpha_{Lk} \right) \tag{5}$$

Mixture enthalpy (static):

$$h = \sum_k Y_k h_k = \sum_k \left(Y_{Vk} h_{Vk} + Y_{Lk} h_{Lk} \right) \tag{6}$$

Mixture specific heat under constant pressure:

$$c_P = \sum_k Y_k c_{Pk} = \sum_k \left(Y_{Vk} c_{PVk} + Y_{Lk} c_{PLk} \right) \tag{7}$$

Mixture dynamic viscosity:

$$\frac{1}{\mu} = \sum_k \left(\frac{\alpha_{Vk}}{\mu_{Vk}} + \frac{\alpha_{Lk}}{\mu_{Lk}} \right) \tag{8}$$

The above equation has as main characteristic that mixture dynamic viscosity does not go to infinity when solid phase is present. Mixture viscosity in the presence of solid phase is an open area of research, see e.g. Cheng and Law (2003).

Mixture thermal conductivity:

$$\lambda = \sum_k \left(Y_{Vk} \lambda_{Vk} + Y_{Lk} \lambda_{Lk} \right) \tag{9}$$

3.3 Mixture and slip velocity definitions

Mixture velocity (mass averaged) is defined by:

$$\vec{U} \equiv \sum_k \left(Y_{Vk}\vec{U}_{Vk} + Y_{Lk}\vec{U}_{Lk} \right) \tag{10}$$

By definition the slip velocity is defined as the relative velocity of the non-vapour phase with respect to the prevailing vapour phase. Then, for component-k we have:

$$\vec{U}_{Sk} \equiv \vec{U}_{Lk} - \vec{U}_V \tag{11}$$

An averaged over all components non-vapour phase velocity may be defined as following:

$$\vec{U}_L \equiv \frac{\sum_k Y_{Lk}\vec{U}_{Lk}}{Y_L} \quad , \quad Y_L \equiv \sum_k Y_{Lk} \tag{12}$$

Similarly an averaged slip velocity may be defined as:

$$\vec{U}_S \equiv \frac{\sum_k Y_{Lk}\vec{U}_{Sk}}{Y_L} = \vec{U}_L - \vec{U}_V \tag{13}$$

Then the mixture mass averaged velocity of eq. (10), takes the following forms:

$$\vec{U} = \sum_k \left(Y_{Vk}\vec{U}_V + Y_{Lk}\vec{U}_{Lk} \right) = \vec{U}_V + \sum_k Y_{Lk}\vec{U}_{Sk} = \vec{U}_V + Y_L\vec{U}_S \tag{14}$$

Often the drift velocity is introduced instead of the slip velocity. By definition the drift velocity is defined as the relative velocity of the non-vapour phase with respect to the mixture. Then, for component-k non-vapour phase we have:

$$\vec{U}_{Dk} \equiv \vec{U}_{Lk} - \vec{U} \tag{15}$$

3.4 Mean flow conservation equations

The basic mean flow conservation equations in vector form, appropriately averaged for turbulent flow, but including the molecular diffusive transport contributions, are presented below.

3.4.1 Mixture Mass

Mixture mass conservation:

$$\frac{\partial \rho}{\partial t} + \nabla \cdot \left(\rho \vec{U} \right) = 0 \tag{16}$$

3.4.2 Component mass

Component-k vapour phase mass conservation:

$$\frac{\partial \rho Y_{Vk}}{\partial t} + \nabla \cdot \left(\rho \vec{U} Y_{Vk} \right) = -\nabla \cdot \vec{J}_{Vk} + \Gamma_{vap,k} - \Gamma_{con,k} + S_{Y_{Vk}}^{Slip} \tag{17}$$

With Γ_{vap} and Γ_{con} being the vaporization and condensation mass fluxes and S^{Slip} the source associated with slip.

Component-k non-vapour phase mass conservation:

$$\frac{\partial \rho Y_{Lk}}{\partial t} + \nabla \cdot \left(\rho \vec{U} Y_{Lk} \right) = -\nabla \cdot \vec{J}_{Lk} - \Gamma_{vap,k} + \Gamma_{con,k} + S_{Y_{Lk}}^{Slip} \tag{18}$$

Component-k total mass conservation results by summing the two equations above:

$$\frac{\partial \rho Y_{k}}{\partial t} + \nabla \cdot \left(\rho \vec{U} Y_{k} \right) = -\nabla \cdot \left(\vec{J}_{Vk} + \vec{J}_{Lk} \right) + S_{Y_{k}}^{Slip} \tag{19}$$

$$S_{Y_k}^{Slip} = S_{Y_{Vk}}^{Slip} + S_{Y_{Lk}}^{Slip} \tag{20}$$

$$\vec{J}_{Vk} = -\left(\frac{\mu_t}{Sc_t} + \rho D_{Vk} \right) \nabla Y_{Vk} \tag{21}$$

$$\vec{J}_{Lk} = -\left(\frac{\mu_t}{Sc_t} + \rho D_{Lk} \right) \nabla Y_{Lk} \tag{22}$$

Note that the vapour and non-vapour component-k mass conservation equations have the same volumetric vaporization / condensation terms in the right hand side, but with opposite signs, so these terms cancel each other in the total mass conservation for component-k.

Finally, if we add the total mass conservation equations (19) for all components we should be able to reproduce the mixture mass conservation eq. (16). Therefore the following compatibility requirement should apply:

$$\sum_k \left(D_{Vk} \nabla Y_{Vk} + D_{Lk} \nabla Y_{Lk} \right) = 0 \tag{23}$$

3.4.3 Mixture Momentum

$$\frac{\partial \rho \vec{U}}{\partial t} + \nabla \cdot \left(\rho \vec{U} \vec{U} \right) = -\nabla \mathrm{P} + \nabla \cdot \left(\tilde{\tau} \right) + \rho \vec{g} + S_U^{Slip} \tag{24}$$

$$\tilde{\tau} = \left(\mu + \mu_t \right) \left(\nabla \vec{U} + \nabla \vec{U}^T \right) - \frac{2}{3} \tilde{\delta} \left(\rho k + \mu \nabla \cdot \vec{U} \right) \tag{25}$$

3.4.4 Mixture Energy (static enthalpy)

$$\frac{\partial \rho h}{\partial t} + \nabla \cdot \left(\rho \vec{U} h \right) = \frac{dP}{dt} - \nabla \cdot \vec{q} - \nabla \cdot \sum_k \left(\vec{J}_{Vk} h_{Vk} + \vec{J}_{Lk} h_{Lk} \right) + S_h^{Slip} \tag{26}$$

$$\vec{q} = -\left(\frac{c_P \mu_t}{\mathrm{Pr}_t} + \lambda \right) \nabla T \tag{27}$$

3.5 Homogeneous Equilibrium Mixture approach

Under the homogeneous equilibrium mixture (HEM) approach all phases and components are assumed to share the same velocity and same temperature, i.e. mechanical and thermal equilibrium is assumed to exist. Under these conditions all slip source terms introduced in the conservation equations above are zero.

According to Lagumbay et al. (2007) in the HEM approach: "the phases and/or components are assumed to be sufficiently well mixed and the disperse particle size are sufficiently small thereby eliminating any significant relative motion. The phases and/or components are strongly coupled and moving at the same velocity. In addition, the phases and/or components are assumed in close proximity to each other so that heat transfer between the phases and/or components would occur at small time-scale maintaining the phases and/or components in thermodynamic equilibrium. Furthermore, the response of the disperse phase (e.g., response of bubbles in the liquid) to the change in pressure is assumed an essentially instantaneous change in their volume so that the disperse phase would behave quasi-statically and the mixture would be in constant pressure. The frequency disturbance of the disperse phase is assumed smaller than the natural frequencies of the disperse phase themselves in order to maintain thermodynamic equilibrium."

3.6 Homogeneous Non-Equilibrium Mixture approach

Under the homogeneous non-equilibrium mixture approach (HNEM) mechanical and/or thermal non-equilibrium is assumed between phases/components.

3.6.1 Mechanical non-equilibrium

Under the mechanical non-equilibrium assumption vapour phase is usually assumed to have same velocity for all components, while non-vapour phase of each mixture component is assumed to have its own velocity different from the common vapour phase velocity.

The slip terms in the conservation equations take the following form:

$$S_{Y_{Lk}}^{Slip} = \nabla \cdot \left[\rho Y_{Lk} \left(Y_L \vec{U}_S - \vec{U}_{Sk} \right) \right] \tag{28}$$

$$S_{Y_{Vk}}^{Slip} = \nabla \cdot \left[\rho Y_{Vk} Y_L \vec{U}_S \right] \tag{29}$$

$$S_{Y_k}^{Slip} = \nabla \cdot \left[\rho \left(Y_k Y_L \vec{U}_S - Y_{Lk} \vec{U}_{Sk} \right) \right] \tag{30}$$

$$S_U^{Slip} = -\nabla \cdot \left(\rho Y_L \left(1 - Y_L \right) \vec{U}_S \vec{U}_S \right) \tag{31}$$

$$S_h^{Slip} = \nabla \cdot \left[\rho Y_L \vec{U}_S \left(h - h_L \right) \right] - Y_L \vec{U}_S \left(1 - \frac{\rho}{\rho_L} \right) \nabla P \tag{32}$$

Where mixture non-vapour enthalpy and density are defined as:

$$h_L Y_L \equiv \sum_k \left(Y_{Lk} h_{Lk} \right)$$
$$\frac{Y_L}{\rho_L} \equiv \sum_k \left(\frac{Y_{Lk}}{\rho_{Lk}} \right) \quad (33)$$

3.6.2 Thermal Non-Equilibrium

Under the thermal non-equilibrium assumption vapour and liquid states are assumed to have different temperatures.

Thermodynamic non-equilibrium physically occurs when changes in the flow are much faster than the time needed by the phases to exchange heat and mass and reach equilibrium. Thermodynamic non-equilibrium is expected to be related to phenomena such as expansion of under-expanded jets near the exit nozzle see Lyras et al. (2018) and Kim et al. (2009), RPT (rapid phase transition) and BLEVE (boiling liquid expanding vapour explosion).

Thermodynamic non-equilibrium CFD simulations with hydrogen have not been reported. Thermodynamic non-equilibrium has been considered within 0d integral hydrogen release modelling see next chapter.

3.7 Phase change

Phase change below focuses on vaporization/condensation phenomena, i.e. phase changes between liquid and vapour, but the model formulations presented could also be considered as representing phase changes between solid and vapour, which are encountered in CO_2 dispersion for example (sublimation and deposition). Phase changes between solid and liquid (freezing and melting) e.g. when humidity is accounted for during cryogenic hydrogen dispersion or when dry air is considered as a mixture of N_2 and O_2 are examined in a separate section.

Computational modelling of phase change in flash boiling single component flows has been reviewed by Liao and Lucas (2017).

3.7.1 Implicit modelling of vaporization / condensation (ADREA-HF)

In ADREA-HF code vaporization / condensation phenomena are modelled implicitly. ADREA-HF first solves the mixture enthalpy and component total mass fraction conservation equations, both of which do not contain phase change terms. Then phase distribution and mixture temperature are calculated from mixture enthalpy, pressure and component total mass fractions by application of Raoult's equilibrium law for ideal mixtures (see eq. 34 below). This procedure is often referred to in the literature as a Ph-flasher (h stands for enthalpy). If temperature is known instead of enthalpy, the procedure is known as a PT-flasher. Once the phase distribution of a given component is known, then eq. (17) or eq. (18) can be used to calculate the respective volumetric total phase change rate.

The Ph-flasher in ADREA-HF is an iterative procedure over mixture temperature, where a PT-flasher is applied per iteration until the correct mixture enthalpy is attained. The PT-flasher consists in applying Raoult's law for ideal mixtures for each of the mixture components, and solving the resulting system of equations. In ADREA-HF this system is solved using the conventional Rachford-Rice procedure, but more complex approaches also exist, see Michelsen (1994) and the topic is still an open area of research.

Raoult's law for ideal mixtures expresses the fact the under thermodynamic equilibrium, partial pressure of component k in the vapour phase balances the vapour pressure (surface tension) of component k in the liquid phase:

$$\frac{Y_{Vk}/M_k}{\sum_k Y_{Vk}/M_k} P = \frac{Y_{Lk}/M_k}{\sum_k Y_{Lk}/M_k} P_{Sat,k}(T) \tag{34}$$

The coefficients of the pressures in the above relation are the molar fractions of component-k in the vapour and liquid phases. The expression for the partial pressure of component-k in the vapour phase on the left hand side follows from Dalton's law.

Since phase distribution calculations can be computationally expensive, criteria are usually applied for phase change appearance, based on mixture dew (or bubble) pressure or temperature. More specifically, two-phase conditions will exist when the mixture pressure is below the mixture bubble pressure and above the mixture dew pressure. Equivalently, two-phase conditions will exist when the mixture temperature is below the mixture dew temperature and above the mixture bubble temperature.

In the most simple case of a binary mixture of air and one additional component (e.g. hydrogen), where air is considered to have a constant composition and remain always in the gaseous state (infinite value of vapour pressure), while the additional component can be in two-phase conditions, it can be shown that eq. (34) results in the following phase distribution:

$$Y_L = \frac{Y - Y_{Sat}}{1 - Y_{Sat}}, \quad Y_V = Y - Y_L \tag{35}$$

$$Y_{Sat} = \frac{1}{1 + \left(\frac{P}{P_{Sat}(T)} - 1 \right) \frac{M_{Air}}{M}} \tag{36}$$

The above formulae state that hydrogen in liquid phase will exist only if hydrogen total mass fraction is greater than the saturated value of hydrogen total mass fraction in the mixture eq. (36), which as observed depends on pressure and temperature.

3.7.2 Explicit modelling of vaporization / condensation (FLUENT)

Hydrogen vaporization/condensation phenomena for a binary mixture of air and two-phase hydrogen were modelled by Jin et al. (2017) using FLUENT code.

A conservation equation was solved for total mass fraction of hydrogen and a separate conservation equation for the vapour mass fraction of hydrogen with the following phase change source terms, according to Lee (1979).

$$\Gamma_{vap} = c\rho Y_L \max\left(\frac{T_L - T_{Sat}}{T_{Sat}}, 0 \right) \tag{37}$$

$$\Gamma_{con} = c\rho Y_V \max\left(-\frac{T_V - T_{Sat}}{T_{Sat}}, 0 \right) \tag{38}$$

The vaporization term is activated if liquid hydrogen is present and its temperature is found above the saturation temperature of hydrogen at the given mixture pressure. The condensation term is activated if vapour hydrogen is present and its temperature is found below the saturation temperature of hydrogen. The above Lee (1979) model is a non-equilibrium model as long as different temperatures are used for hydrogen liquid and vapour. Jin et al. (2017) used the above model by assuming thermodynamic equilibrium, i.e. hydrogen vapour and liquid are both at the mixture temperature.

The value of the coefficient c was reported to be 0.25 (s^{-1}), tuned by comparing simulations against the NASA experiments of Witcofski and Chirivella (1984).

The inverse of c can be considered as a relaxation time and the model as a relaxation model in the sense that it accounts for a time delay to obtain saturated conditions.

3.7.3 Explicit modelling of vaporization / condensation (FLACS)

For a binary mixture of air and two-phase hydrogen FLACS development code solves mass conservation equations for mixture fractions of vapour phase and liquid phase of hydrogen, which include phase change terms, see Ichard et al. (2012). According to Mauri (2019) these source terms take the following form, in terms of the mass fraction formulation used in this work:

$$\Gamma_{vap} = \rho \max\left(\frac{Y_V^* - Y_V^t}{\Delta t}, 0\right) \tag{39}$$

$$\Gamma_{con} = \rho \max\left(\frac{Y_L^* - Y_L^t}{\Delta t}, 0\right) \tag{40}$$

Superscript (*) refers to time t+dt, but only due to phase change, while superscript (t) to values at the previous time integration step. The starred variables and therefore the phase change are calculated assuming that a) phase change and transport as separate sequential processes b) phase change is an isenthalpic process, i.e. hydrogen mass and mixture static enthalpy are preserved from time t to time t+dt and c) Raoult's equilibrium law holds at time t+dt. These assumptions lead to the relations below, where the saturated value of hydrogen total mass fraction is taken from eq. (35). After substitution of eqs (41), eq. (42) is solved iteratively for the mixture temperature.

$$Y_L^* = \frac{Y^t - Y_{Sat}\left(T^*\right)}{1 - Y_{Sat}\left(T^*\right)}, \quad Y_V^* = Y^t - Y_L^*, \quad Y_{air} = 1 - Y^t \tag{41}$$

$$Y_{air}h_{air}\left(T^*\right) + Y_V^* h_V\left(T^*\right) + Y_L^* h_L\left(T^*\right) = Y_V^t h_V\left(T^t\right) + Y_L^t h_L\left(T^t\right) + Y_{air}h_{air}\left(T^t\right) \tag{42}$$

3.7.4 Explicit modelling of vaporization / condensation (GASFLOW-MPI)

GASFLOW-MPI (2016) uses a thermal non-equilibrium model developed for the phase change modelling of steam and liquid water in which different temperatures for each phase are calculated using two energy equations one for the gaseous phase and one for the liquid droplets. In this model condensation and vaporization source terms are as following:

$$\Gamma_{vap} = c \max\left[\rho Y_V - \rho_{V,sat}\left(P_{sat}, T_V\right), 0\right] \tag{43}$$

$$\Gamma_{con} = c \max\left[\rho_{V,sat}\left(P_{sat}, T_V\right) - \rho Y_V, 0\right] \tag{44}$$

The relaxation coefficient, c, which has the unit of inverse time, can be written as:

$$c = 6\frac{D_{V\to L}}{d_L^2}\mathrm{Sh} = 6\frac{D_{V\to L}}{d_L^2}\left[2 + 0.6\cdot\left(\mathrm{Sc}\cdot\mathrm{Re}\right)^{\frac{1}{3}}\right] \tag{45}$$

Sh is the Sherwood number which is calculated as function of Schmidt number, Sc, and Reynolds number, Re. $D_{V\to L}$ is the mass diffusion coefficient of vapour into dispersed liquid droplets which is the molecular mass diffusion coefficient plus the turbulent effects.

The transport equation of the liquid droplet diameter, d_L, is given as:

$$\frac{\partial}{\partial t} d_L + \vec{U}_L \cdot \nabla d_L = \frac{d_L}{3} \frac{\left(\Gamma_{con} - \Gamma_{vap}\right)}{\rho Y_L} \tag{46}$$

The above phase change model is planned to be extended for vapour and liquid hydrogen within PRESLHY project.

3.7.5 Freezing / melting phenomena

In ADREA-HF code solid phase of component-k appears when mixture temperature falls below freezing temperature of component-k.

3.8 Slip velocity modelling / Rainout

Slip between phases is the physical mechanism of rainout which results to pool formation. Theoretically speaking, without slip, i.e. assuming mechanical equilibrium, the non-vapour phase can still approach the ground (solid surface), due to gravity or impingement, but will never be on the ground itself.

A relatively simple method to calculate slip velocities is using algebraic slip modelling. Such a method was used by Giannissi et al. (2014) to account for slip of hydrogen and water droplets. Algebraic slip modelling was also used by Liu et al. (2018).

A far more complex approach is to solve extra momentum conservation equations for the liquid phase, which include source terms to account for drag between the phases plus other source terms see Manninen et al (1996). Such an approach was used by Giannissi and Venetsanos (2018) to account of slip of hydrogen, humidity, oxygen and nitrogen.

Both approaches required assumptions regarding droplet diameter sizes either assumed droplet sizes or assumed droplet size distributions.

Slip velocity modelling generally requires information about droplet diameter sizes see Witlox and Bowen (2002). Once droplet sizes are known at the source, either from mechanical breakup or flashing criteria/correlations, then their evolution (vaporization) within the flow can be tracked using droplet population conservation equations for the component released at the source (hydrogen). For humidity, oxygen and nitrogen that could condense or freeze due to a cryogenic hydrogen release the source is not spatially at a fixed location, therefore the respective droplet population equations should include droplet formation (nucleation) terms, which may require complex modelling.

Ichard et al. (2012) used a special slip/rainout model to produce pool formation, in which droplet sizes is not a required input. Rain-out is authorized only if the temperature of the mixture inside the computational cell adjacent to the wall is less than or equal to the normal boiling point of the mixture which indicates that liquid is evaporating and that thermodynamic equilibrium has been reached. Then liquid is removed from the flow (and injected inside the pool) for distances from solid less than a critical rainout length scale, which is defined as the product of the characteristic velocity scale for rainout and the characteristic time scale for the rainout process. Appropriate source terms are integrated inside the transport equations for the mixture fractions and mixture enthalpy. The characteristic time scale over which the rain-out process occurs is assumed to be the time needed by the flow to achieve a new thermodynamic equilibrium in the computational cell adjacent to the wall. The characteristic velocity for the rainout process is taken to be the local maximum velocity

in regions of the flow where liquid is evaporating and thermodynamic equilibrium has been attained.

3.9 Turbulence

Classical RANS turbulence models, such as standard k-ε, RNG- k-ε or others have been originally developed for single phase, single component flows.

One simple approach of treating turbulence within the homogeneous mixture approach is to apply a classical RANS model with the mixture as the working fluid, and neglect the effects of non-vapour phase on turbulence. Such an approach has been used in the past by Venetsanos and Bartzis (2007), Giannissi and Venetsanos (2018) as well as Venetsanos et al. (2019). An alternative approach is to use the mixture vapour phase as working component of a classical RANS model.

Non-vapour phase (liquid droplets and / or solid particles) dispersed into the gaseous phase may affect turbulence, the effect depending on the size of droplets/particles and their velocity with respect to the vapour phase. According to Garcia and Crespo (2000) large particles generate turbulence while small particles suppress it, the transition occurring when the particle size is about 1/10 of the integral length scale of turbulence.

More specifically, for dilute gas particle flows and small Stokes number (mean velocity of particles very similar to that of the gaseous phase) Garcia and Crespo (2000) used the classical k-ε model for the gaseous phase, modified with additional terms in the k and ε conservation equations. For all experiments analyzed they found that the particles increased the dissipation of turbulent kinetic energy.

For turbulence / particle interaction the reader can also see Brennen (2002).

Regarding turbulent Prandt and Schmidt numbers entering the conservation equations the most common approach is to assume them both constant and equal to 0.72. Other formulations accounting for stability effects exist but these have not yet been tested for hydrogen dispersion.

3.10 Boundary conditions

3.10.1 Ground

The effect of the ground heat transfer in cryogenic dispersion is important see Verfondern and Dienhart (1997) as well as Statharas et al. (2000).

The integration domain of the conservation equations given in the previous sections starts either directly from the ground if a pool is not directly modelled or from the pool external surface, if a pool is modelled and the pool has been formed. For more on pool modelling see next chapter. In both cases cryogenic hydrogen dispersion over ground requires solving the unsteady energy equation inside the ground (usually in one-dimensional form) in order to determine the ground temperature distribution and the ground heat flux. The ground energy equation is solved down to an assumed underground level where usually temperature is assumed constant and unaffected by the cryogen dispersion.

In case a pool is not modelled heat flux consistency is applied as a boundary condition at the interface between ground and the ambient. The heat flux from the ambient side is usually calculated from forced or mixed (forced and natural) convection wall functions / correlations that connect interface temperature with temperature at the adjacent to the ground computational cell. In case of liquid hydrogen present in the adjacent cell, it may be necessary to augment heat transfer coefficient in order to account for boiling. The heat flux from the ground side is obtained from the calculated ground temperature distribution.

A systematic evaluation of the ambient heat transfer coefficient correlations for cryogenic dispersion is an open issue.

3.10.2 Hydrogen jet source

Flow and thermodynamic conditions at the jet source are calculated using release models and in case of under-expanded jets notional nozzle modelling, see next chapter.

Once the jet source conditions are known, then they can be implemented either as volumetric source terms in the conservation equations, or as boundary conditions at computational cell faces, see Tolias et al. (2017).

A systematic evaluation of the above two approaches has not yet been performed for both non-cryogenic and cryogenic dispersion and therefore is an open issue.

4 Integral modelling approaches

4.1 Release modelling

Release calculations are performed employing 0d models that connect stagnation conditions with conditions at the nozzle exit, through mass, momentum and energy principles. In order to determine whether flow at the nozzle exit is choked or not an additional flow maximization algorithm (or condition) is also required.

Homogeneous equilibrium two-phase choked flow modelling using the Helmholtz free energy based EoS of Leachman et al. (2009) was reported by Houf and Winters (2013) and Venetsanos and Giannissi (2017).

Homogeneous non-equilibrium two-phase choked flow modelling using the Leachman et al. (2009) EoS was reported by Travis et al. (2012) and by Venetsanos (2018).with validation performed against the NASA experiments of Simoneau and Hendricks (1979).

One dimensional modelling of the steady state choked flow through a discharge line of variable cross section was considered by Venetsanos (2019). The model solves the mass, momentum and energy balance equations and finds choked flow using PIF algorithm. For the flashing inside the discharge line, three modelling approaches were implemented, the Homogeneous Equilibrium Model (HEM) and two non-equilibrium models: Homogeneous Relaxation Model (HRM) and Delayed Equilibrium Model (DEM). Physical properties are calculated based on Leachman et al. (2009) EoS. Given the current absence of relevant hydrogen data, preliminary validation work was performed against experimental data from the old Super Moby Dick experiments with water, while future validation will be based on the discharge experiments performed within PRESLHY.

Gaseous choked flow modelling using the Leachman et al. (2009) EoS was reported by Xiao et al. (2011).

Gaseous release modelling with Abel-Noble EoS has been reported by Schefer et al. (2007) and Molkov et al. (2009). Cirrone et al., (2019a) used the model by Molkov et al. (2009) to estimate the release sources for cryogenic hydrogen jets. Results on the mass flow rate were compared to over 100 experimental tests conducted at Sandia National Laboratories and reported in Panda and Hecht (2017), Hecht and Panda (2016, 2018). The release temperature and pressure were maintained constant during each test. Release temperature was included in the range 37-295 K and pressure varied within the range 2-6 bar abs. Three nozzle diameters were employed for the experiments: 0.75, 1, 1.25 mm. Release parameters were monitored in the pipe upstream the interchangeable orifice and assumed as stagnation conditions in calculations. It was verified that velocity of the flow in the pipe would cause an associated dynamic pressure less than 0.01% the static pressure, confirming the validity of the stagnation conditions assumption.

The release conditions are all located in the vapour/gas phase. Even in the possible worst-case scenario, i.e. coupling the lowest release temperature (46 K) and the highest pressure (6 bar), an isentropic expansion to ambient pressure does not cross the saturation curve.

The mass flow rate calculated using the Abel Noble EoS was compared to the mass flow rate evaluated employing NIST EoS. In the latter case, the exit conditions were iteratively calculated gradually decreasing temperature along the isentropic expansion transformation from the “storage” conditions to the real nozzle until the equation of energy conservation was satisfied. This procedure was applied to 39 tests of the entire set of available experiments. It was found that the maximum variation in the mass flow rate calculated with NIST EoS was 7% and it was given, as expected, for the release at the lowest temperature (46 K). Therefore, it is confirmed that for pressures up to 6 bar abs, the two EoSs can be used interchangeably without affecting significantly the resulting release mass flow rate for the considered range of temperature.

Figure 3 compares the calculated mass flow rate against experiments. In 77 tests, indicated as d=1.00 mm* in Figure 3, release temperature was retrieved graphically from a chromatic legend and not from exact values (Hecht and Panda, 2016). It is estimated that the inaccuracy in the release

temperature approximation is maximum ±10K. Such inaccuracy in temperature can lead up to 10% relative difference in the mass flow rate calculation for the lowest release temperature (37 K). The relative difference is observed to decrease with the increase of release temperature to 7% and 5% for T=65 K and T=95 K respectively. Deviation of calculated mass flow rate from experiments is contained within ±10% with the exception of a test with T=37 K and P=2 bar abs (deviation 23%). This test may be affected by the accuracy in retrieving graphically the release temperature. Following the general good agreement between calculated mass flow rate and experiments, it is concluded that the theory can be used to calculate the flow conditions at the nozzle exit and mass flow rate for hydrogen jets with temperature in the range 37-295 K and pressure up to 6 bar abs.

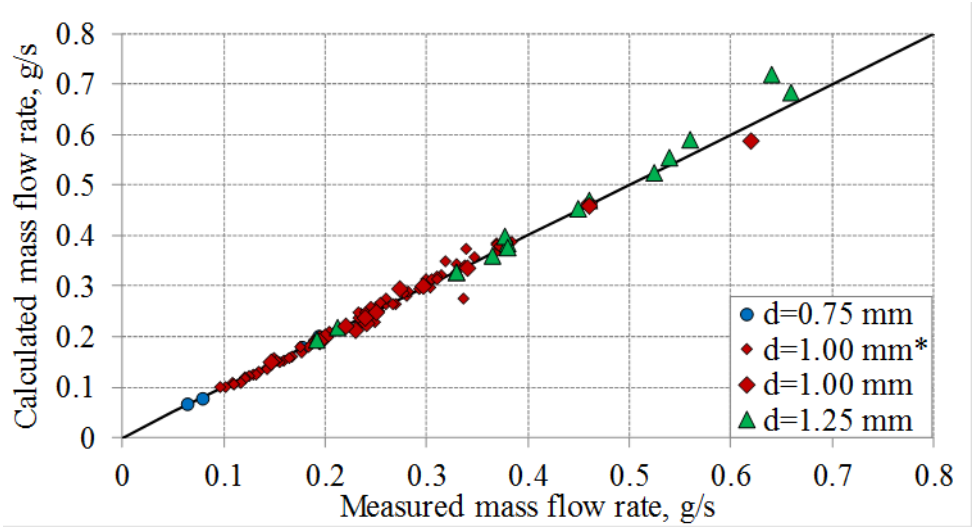

Figure 3 Calculated versus experimental mass flow rate.

4.2 Notional nozzle approach

The notional nozzle approach originates from studies related to under-expanded non-cryogenic jets of natural gas see Birch et al. (1984). A release from a pressurized gaseous hydrogen storage tank at pressure above 2 bar can produce an under-expanded jet. At the real nozzle exit velocity is locally sonic, and pressure is above atmospheric. Consequently, the gas must expand outside the real nozzle, forming a shock structure while reaching the ambient pressure upstream of the Mach disk.

CFD simulations examining the structure of the expansion of under-expanded non-cryogenic jets have been reported elsewhere, e.g. by Khaksarfard et al. (2010) and Hamzehloo and Aleiferis (2014).

Experiments involving under-expanded cryogenic hydrogen jets have been performed by different research groups, e.g. by Veser et al. (2011), Friedrich et al. (2012) and more recently by Hecht and Panda (2018).

Notional nozzle modelling approaches are 0d integral models that connect conditions at the nozzle exit with expanded conditions at the notional nozzle, in order to either provide source boundary conditions for CFD or 1d integral jet-plume models or to provide suitable source parameters for jet / plume similarity laws (see next chapter).

In general conditions at the nozzle are connected to conditions at the notional nozzle through mass, momentum and energy principles. All approaches below (except if mentioned) assume a) mass balance between nozzle exit and notional nozzle, b) no mass transfer with the ambient air during the expansion, c) uniform conditions across both the nozzle exit and the notional nozzle and d) pressure is atmospheric at notional nozzle.

Depending on the assumptions adopted regarding momentum and energy, the various approaches can be classified as shown in Table 2.

The first three approaches determine the notional nozzle velocity assuming a Mach equal to one condition at the notional nozzle, which is assumed located exactly at the Mach disk, where experimental evidence suggests that Mach equals to one.

Notional nozzle temperature was assumed equal to the ambient by Birch et al. (1984) implying that heating occurs during the expansion (either from the existence of shocks or from the surrounding ambient air).

Notional nozzle temperature was assumed equal to the temperature at the nozzle exit by Ewan and Moodie (1986) implying an isothermal expansion.

Molkov et al. (2009), see also Molkov (2012), assumed that the transition from nozzle to notional nozzle is adiabatic. Such a condition implies that the total enthalpy at the nozzle is equal to that at the notional nozzle. The behaviour of notional nozzle temperature for the Molkov et al. (2009) model will be assessed below by examining specific examples.

The next four approaches, all determine the notional nozzle velocity by applying momentum balance between nozzle and notional nozzle. Such an assumption usually leads to supersonic velocities at the notional nozzle for non-cryogenic releases. The level of the Mach number will be assessed below by examining specific examples.

Birch et al. (1987) proposed to set the temperature at the notional nozzle equal to the ambient. The same approach was used later by Schefer et al. (2007) with different EoS formulation.

Venetsanos and Giannissi (2017), see also Giannissi et al. (2019), proposed to set the temperature at the notional nozzle equal to the nozzle temperature.

Determination of the notional nozzle temperature assuming adiabatic energy balance (constant total enthalpy) has been reported by Yuceil and Otugen (2002) and Witlox and Bowen (2002). According to Witlox and Bowen (2002) this model corresponds to that included in the integral codes HGSYSTEM and PHAST and also to the formulation recommended by Britter (1994 and 1995), while in order to avoid excessive post-expansion velocities for cases where turbulence becomes important, PHAST adopts a rather arbitrary cut-off velocity of the velocity. The adiabatic energy balance approach was applied for cryogenic hydrogen by Xiao et al. (2011), Houf and Winters (2013) and Giannissi et al. (2019). According to Witlox and Bowen (2002),

Finally, the last entry in Table 2 shows the additional option of determining the notional nozzle temperature by assuming constant entropy between nozzle and notional nozzle. This isentropic model should be considered as a limiting case, since entropy is expected to increase between nozzle and notional nozzle. According to Witlox and Bowen (2002) this model was adopted in the TNO Yellow Book (1979).

Table 2: Notional nozzle models basic assumptions

Model id	Mach=1	Momentum balance	Adiabatic	Ambient temperature	Isothermal	Isentropic
1	√			√		
2	√				√	
3	√		√			
4		√		√		
5		√			√	
6		√	√			
7		√				√

In addition to the notional nozzle modelling approaches included in Table 2, Harstad and Bellan (2006) proposed to locate the notional nozzle beyond the Mach disk, with a Mach number lower than one there. Li et al. (2015) proposed a special two-layer approach, which includes partitioning

of the flow between the central core jet region leading to the Mach disk and the supersonic slip region around the core. The flow after the Mach disk is subsonic while the flow around the Mach disk is supersonic with a significant amount of entrained air. The predictions of this model were compared to previous experimental data for high pressure non-cryogenic hydrogen jets up to 20 MPa and to notional nozzle models and CFD models for pressures up to 35 MPa. The results showed that this model gives better predictions of the mole fraction distributions than previous models for highly under-expanded jets.

An evaluation of selected notional nozzle approaches for CFD simulations of free-shear under-expanded non-cryogenic hydrogen jets has been performed by Papanikolaou et al. (2012). Comparing the various notional nozzle approaches, it was found that these could be grouped based on the momentum and energy flux at the source with Birch et al. (1987) and Schefer et al. (2007) generally performing better, followed by Birch et al. (1984) and Ewan and Moodie (1986) and lastly Harstad and Bellan (2006). The Yuceil and Otugen (2002) approach was not considered in the performed CFD simulations, but this approach preserves both momentum and energy flow rates, besides mass.

A comparison of the notional nozzle approaches of Table 2 is performed below in terms of predicted conditions at the notional nozzle, for nozzle diameter of 1 mm, hydrogen stagnation pressure of 10 MPa, ambient conditions 1 atm, 293.15 K and stagnation temperatures covering both non-cryogenic and cryogenic conditions.

Calculated nozzle conditions are shown in Table 3. All release and notional nozzle calculations below have been performed with a tool developed by NCSRD for use within the NET-TOOLS elab platform, based on Venetsanos and Giannissi (2017) and Venetsanos (2018), tool which calculates hydrogen physical properties using the Leachman et al. (2009) EoS formulation. Table 3 shows as expected that, for given stagnation pressure and nozzle diameter, hydrogen mass flow rate increases with lowering the stagnation temperature.

Table 3: Predicted nozzle conditions for nozzle diameter 1 mm, hydrogen stagnation pressure 10 MPa and various stagnation temperatures

Stagnation temperature (K)	Mass flow rate (g/s)	Velocity (m/s)	Pressure (MPa)	Temperature (K)	Vapour quality	Density (kg/s)
293.15	4.853	1235.99	5.15	241.46	1	5.000
80	10.988	674.79	4.20	58.39	1	20.733
50	18.163	566.32	2.35	36.77	1	40.835

Notional nozzle results for stagnation temperature of 293.15 K are shown in Table 4 and Figure 4. Regarding the models 1-3, based on the Mach equal to one assumption, it can be observed that they predict comparable notional nozzle diameters, with the highest value predicted by model 1. Notional nozzle conditions predicted by models 2 and 3 are very comparable in this case, with the model 3 notional nozzle temperature slightly higher than the nozzle temperature.

The models based on momentum balance (4-7) all predict supersonic flow and notional diameters lower or even much lower than models 1-3, in this case. The lowest supersonic Mach and largest diameter is predicted by the model 4 and the highest Mach and smallest diameter when using the isentropic assumption (model 7). Additionally, models 6 and 7 predict notional nozzle temperature significantly lower than the nozzle temperature. Finally, as shown in Figure 4, in all cases except the isentropic an entropy increase is predicted between nozzle and notional nozzle. Note that all points marked 1-7 in Figure 4, lie on the constant pressure line P = 1 atm.

Table 4: Effect of notional nozzle model on notional nozzle conditions for nozzle diameter 1 mm, hydrogen stagnation conditions (10 MPa, 293.15 K) and ambient conditions (1 atm, 293.15 K).

Model id	Diameter (mm)	Velocity (m/s)	Temperature (K)	Density (kg/s)	Mach
1	7.52	1304.63	293.15	0.083757	1
2	7.15	1189.37	241.46	0.101683	1
3	7.18	1198.97	245.62	0.099960	1
4	5.99	2052.97	293.15	0.083757	1.57
5	5.44	2052.97	241.46	0.101683	1.73
6	4.17	2052.97	141.74	0.173240	2.19
7	2.76	2052.97	62.25	0.396202	3.15

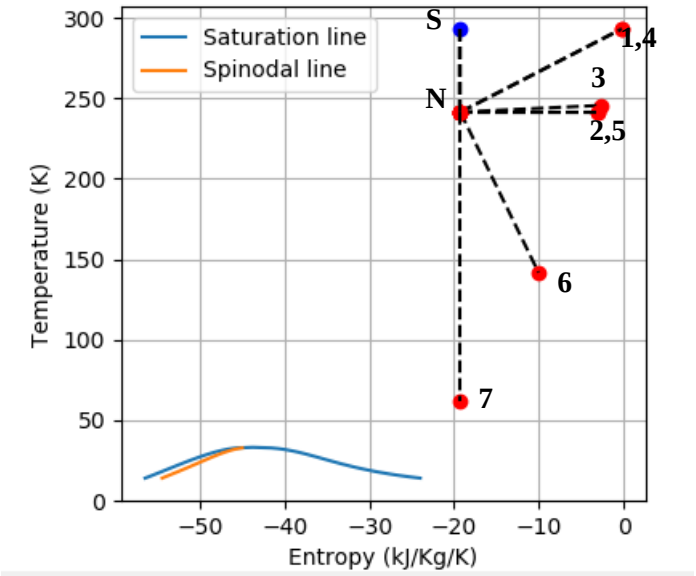

Figure 4 Thermodynamic TS-chart showing hydrogen stagnation conditions (S), nozzle conditions (N) and notional nozzle conditions with the various notional nozzle models (1-7) and for nozzle diameter 1 mm, stagnation conditions (10 MPa, 293.15 K) and ambient conditions (1 atm, 293.15 K)

Notional nozzle results for 80 K stagnation temperature are shown in Table 5 and Figure 5. It can be observed that for the models applying the Mach equal to one condition notional diameters are comparable for models 2 and 3, while model 1 predicts a significantly higher value. Similarly to the previous example, notional nozzle conditions predicted by models 2 and 3 are very comparable, but with the model 3 notional nozzle temperature lower in this case than the nozzle temperature.

Models 5-7 based on momentum balance, all predict supersonic flow and notional diameters lower or even much lower than models 1-3, in this case. In contrast model 4 predicts the largest diameter of all models (1-7) and even subsonic flow at the notional nozzle.

Figure 5 shows the corresponding thermodynamic TS-chart. It seems clear that, for this specific cryogenic release case, models 1 and 4 could be considered as non-physical, due mainly to the very high notional nozzle temperature assumed.

Model 7 is shown to predict liquid phase appearance at the notional nozzle. In this case calculations have been performed using the HEM two-phase flow model. In general for cryogenic under-expanded hydrogen jets the conditions at the nozzle and/or notional nozzle may be in the two-phase regime. Then besides the diameter, velocity and temperature one needs to calculate also the hydrogen vapour mass fraction (vapour quality), which requires an additional assumption regarding the phase change from nozzle exit to the notional nozzle.

Table 5: Effect of notional nozzle model on notional nozzle conditions for nozzle diameter 1 mm, hydrogen stagnation conditions (10 MPa, 80 K) and ambient conditions (1 atm, 293.15 K).

Model id	Diameter (mm)	Velocity (m/s)	Temperature (K)	Density (kg/s)	Mach	Vapour quality
1	11.32	1304.63	293.15	0.083757	1	1
2	7.24	631.84	58.39	0.422858	1	1
3	6.90	577.21	48.74	0.508459	1	1
4	13.14	967.57	293.15	0.083757	0.74	1
5	5.85	967.57	58.39	0.422858	1.53	1
6	3.34	967.57	20.81	1.296105	2.68	1
7	2.82	967.57	20.37	1.815344	3.66	0.729

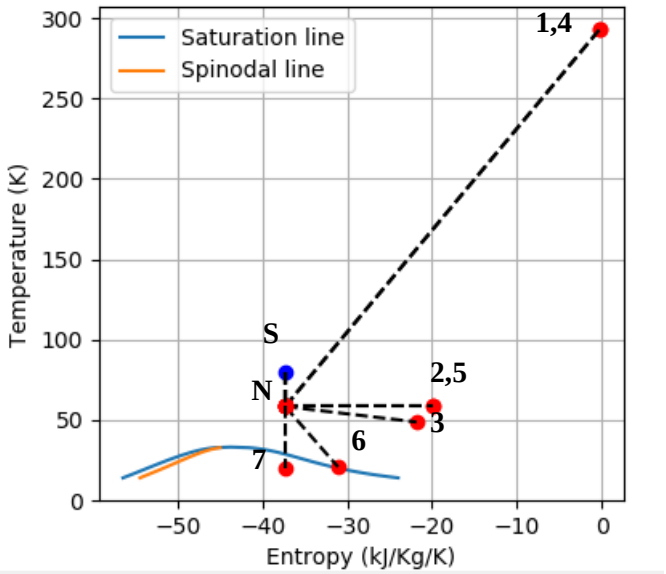

Figure 5 Thermodynamic TS-chart showing hydrogen stagnation conditions (S), nozzle conditions (N) and notional nozzle conditions with the various notional nozzle models (1-7) and for nozzle diameter 1 mm, stagnation conditions (10 MPa, 80 K) and ambient conditions (1 atm, 293.15 K)

Notional nozzle results for 50 K stagnation temperature are shown in Table 6 and Figure 6. Models 1 and 4 considered unphysical for the case with 80 K are also considered unphysical in this case for the same reasons. Their results are shown in Table 6 but not included in Figure 6. It can be observed that in contrast to the previous examples models 2 and 3 now produce not comparable results. Model 3 predicts liquid phase at the notional nozzle, while models 2 and 5 not. Similar to the previous example, two-phase calculations have been performed using the HEM model. Regarding liquid phase appearance at the notional nozzle, it should be noted that models 2 and 5 will never predict liquid phase, even if nozzle conditions are in the two phase regime. Model 3, in contrast has this possibility.

Table 6: Effect of notional nozzle model on notional nozzle conditions for nozzle diameter 1 mm, hydrogen stagnation conditions (10 MPa, 50 K) and ambient conditions (1 atm, 293.15 K).

Model id	Diameter (mm)	Velocity (m/s)	Temperature (K)	Density (kg/s)	Mach	Vapour quality
1	14.55	1304.63	293.15	0.083757	1	1

2	8.25	499.07	36.77	0.681406	1	1
3	7.30	298.32	20.37	1.456340	1	0.913
4	20.40	663.59	293.15	0.083757	0.51	1
5	7.15	663.59	36.77	0.681406	1.33	1
6	3.73	663.59	20.37	2.510747	3.00	0.522
7	3.26	663.59	20.37	3.280463	3.50	0.395

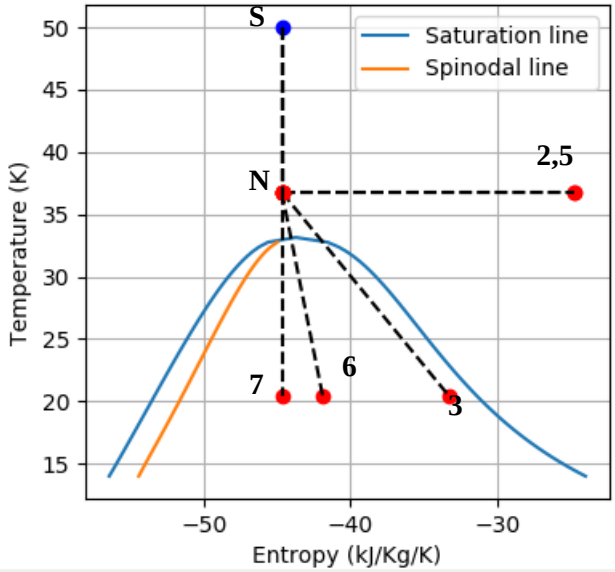

Figure 6 Thermodynamic TS-chart showing hydrogen stagnation conditions (S), nozzle conditions (N) and notional nozzle conditions with the various notional nozzle models and for nozzle diameter 1 mm, stagnation conditions (10 MPa, 50 K) and ambient conditions (1 atm, 293.15 K)

The predictions of the notional models of Table 2 have been inter-compared above, for one non-cryogenic release and two cryogenic ones. All calculations have been performed using very accurate hydrogen physical properties from Leachman et al. (2009). The findings are summarized below.

- Models 1 and 4 should not be applied for cryogenic releases, since they assume un-physically high temperature at the notional nozzle. They could possibly be applied with caution for non-cryogenic releases.
- Model 6 predicted, in all three modelled cases, Mach numbers at the notional nozzle above 2, with tendency to increase with lowering stagnation temperature. For non-cryogenic releases it can produce nozzle temperatures significantly lower than nozzle temperatures.
- Models 3, 6 and 7 are able to produce liquid phase at the notional nozzle, while models 1, 2, 4 and 5 not.
- Models 2 and 3 produce comparable results, when the stagnation temperature is above a certain limit such that model 3 predicted notional nozzle vapour quality is one and non-comparable results below this limit.
- Model 7 is a lower limiting case, since entropy is expected to increase during the expansion to the notional nozzle.

4.3 Pool modelling

Pool modelling provides the boundary conditions required by CFD calculations performed above the pool.

Phenomenology of hydrogen pools can be found in Verfondern (2008). Modelling of spreading and vaporization of liquid hydrogen pools has been reported by Verfondern and Dienhart (1997), using the LAuV code and by Middha et al. (2011) and Ichard et al. (2012), using the FLACS code. In both cases the two-dimensional shallow layer equations are used to model pool spreading.

The shallow layer equations for a boiling pool on horizontal ground are given below. They can be derived by integrating the full three dimensional conservation equations over the layer depth δ, under the main assumption that pressure within the layer is hydrostatic.

The pool mass conservation in conservative form reads:

$$\frac{\partial \rho_L \delta}{\partial t} + \frac{\partial \rho_L \delta u_j}{\partial x_j} = G_{rain} - G_{vap} \tag{47}$$

Here and below j stands for the two horizontal directions x and y. G_{vap} is the mass flux of vapour leaving the pool due to boiling and G_{rain} is the mass flux of liquid feeding the pool due to rainout from the ambient space above the pool.

The pool momentum conservation in conservative form reads:

$$\frac{\partial \rho_L \delta u_i}{\partial t} + \frac{\partial \rho_L \delta u_j u_i}{\partial x_j} = -\frac{g}{2}\frac{\partial \delta^2 \Delta\rho}{\partial x_i} - \tau_w - \tau_\delta + G_{rain} u_{i,rain} - G_{vap} u_i \tag{48}$$

The first term on the right hand side is due to hydrostatic pressure differences, with $\Delta\rho = \rho_L - \rho_a$ being the difference between pool density and ambient density. τ_w is the shear stress between pool and the ground and τ_δ the shear stress between pool and the ambient at the pool top. The last two terms represent the momentum gain or loss of the pool due to rainout and due to boiling.

The pool energy equation in conservative form reads:

$$\frac{\partial \rho_L \delta h_L}{\partial t} + \frac{\partial \rho_L \delta u_j h_L}{\partial x_j} = q_w + q_\delta + G_{rain} h_{rain} - G_{vap} h_V \tag{49}$$

h_L is the pool enthalpy, q_w is the heat flux the pool receives from the ground and q_δ the heat flux heating the pool from the ambient side, which includes convective as well as radiative heating.

For a boiling pool of one component, pool temperature (and consequently pool enthalpy) remains constant equal to the saturation temperature of that component. Therefore, using also eq. (47), the above energy equation can be turned into the following relation for calculating the vaporization mass flux:

$$G_{vap}\left(h_V - h_L\right) = q_w + q_\delta + G_{rain}\left(h_{rain} - h_L\right) \tag{50}$$

The ground heat flux is usually obtained by solving the ground energy equation with given temperature boundary condition, equal to the pool saturation temperature, see also previous chapter. More complex boundary conditions can be formulated at the pool-ground interface, which take into

account the boiling regime (nucleate boiling, transitional boiling and film boiling) from the Nukiyama curve, Verfondern (2010).

Neglecting rainout and ambient heat flux, eq. (50) takes the very simple form below, where L stands for the latent heat for vaporization:

$$G_{vap}L = q_w \tag{51}$$

Liquid hydrogen pools forming on ground after a cryogenic hydrogen release in ambient air, will always be multi-component pools containing liquid hydrogen and solid humid air, i.e. at least solid oxygen, nitrogen and water. LNG pools in contrast will contain only solid water and not solid air.

For pool modelling of LNG releases the reader is directed to Webber et al. (2009) along with Coldrick et al. (2009).

In general, two distinctive cases for pool vaporization are considered: a) boiling and b) evaporation see Fernandez et al. (2012). Cryogenic pools are generally considered to be boiling pools.

At given pressure, the pool will boil when its temperature is at the bubble point, where the bubble temperature, of the mixture, is determined from a flash calculation using Raoult's Law (Wallas, 1985). If pool temperature is below the bubble point, then the pool will evaporate through its interface with the ambient air. For a one component pool, bubble temperature is equal to the saturation temperature of the component at given pressure.

Cavanaugh et al., (1994) defined the rate at which heat must be supplied to the pool for it to remain at the bubble point. If the heat rate supplied to a boiling pool falls below the required, then the pool boiling will stop and the boiling pool will convert to an evaporating pool. The transition from a boiling to an evaporating pool has been accounted for in the integral model of Fernandez et al. (2012).

4.4 Integral models for round turbulent jets

One-dimensional (along the centreline) integral models for round turbulent jets from pressurized cryogenic hydrogen storage have been proposed by Xiao et al. (2011), Houf and Winters (2013) and Giannissi et al. (2019) to predict the hydrogen jet-to-plume trajectory.

The proposed models a) assume Gaussian profiles for mean velocity and density/temperature across the centreline, b) conserve mass, momentum, species and energy along the centreline, and c) use empirical models for ambient air entrainment. Centreline curvature effects, due to buoyancy are accounted for.

The main differences between the models are focused on the entrainment model applied and on whether self-similar Gaussian profiles are applied immediately after the notional nozzle, as in Xiao et al. (2011) or not as in Giannissi et al. (2019) who adopted the approach of Houf and Winters (2013) and considered two intermediate zones between the notional nozzle and the self-similar part: an initial entrainment and heating zone followed by a flow establishment zone.

5 Similarity law for concentration decay in momentum dominated h2 jets

The major risk associated to unignited gaseous hydrogen jets is the formation of a flammable cloud, which constitutes a serious danger of jet fires, deflagration and detonation. Thus, it is of primary interest to have a tool able to evaluate the distances where a dangerous hydrogen concentration in air is achieved, such as the Lower Flammability Limit (LFL) to determine the size of the flammable envelope produced by an unintended hydrogen release.

Chen and Rodi (1980) developed a similarity law for evaluation of the axial concentration decay in momentum-controlled expanded jets, showing that for round jets, the mass fraction C_{ax} at a given distance x is linearly proportional to the orifice diameter d:

$$C_{ax} = 5.4 \sqrt{\frac{\rho_N}{\rho_s}} \frac{d}{x} \tag{52}$$

where ρ_N is the density of hydrogen at the nozzle, ρ_s is the density of the surrounding air and x is the distance from the nozzle. The similarity law formulation for under-expanded jets was attempted by Birch et al. (1984, 1987) and applied to natural gas releases.

5.1 Similarity for non-cryogenic h2 jets (UU)

Shevyakov et al. (1980) conducted theoretical and experimental studies on hydrogen jets, finding a concentration decay constant in close agreement with Chen and Rodi (1980)'s study. Saffers and Molkov (2013) employed the similarity law for momentum-controlled hydrogen jets using Ulster's under-expanded jet theory to calculate density at the nozzle (Molkov et al., 2009). The correlation was validated against experiments on hydrogen jets with release temperature in the range 80-298 K and pressure 2.6-400 bar. Results of a selection of 60 experimental tests from the 302 used for validation, are reported in Figure 7 and compared against the similarity law.

5.2 Similarity for cryogenic h2 jets (UU)

The performance of the similarity law for hydrogen concentration decay in momentum-dominated unignited jets was tested by UU for cryogenic hydrogen releases (Cirrone et al., 2019a). Ulster's under-expanded jet theory was used to calculate flow conditions at the nozzle. Results were compared against 9 experimental tests performed at Sandia National Laboratories (SNL) on releases with pressure 2-5 bar abs and temperature 50-61 K (Hecht and Panda, 2018). It was assessed that all jets are momentum controlled at least up to the distance where hydrogen concentration 4% is reached by verifying that the logarithm of the Froude number for all the tests is above 7 (Molkov, 2012).

Figure 7 shows the comparison between the similarity law and the hydrogen concentration decay measured in experiments. The similarity law well represents the releases through the 1.25 mm diameter nozzle, providing an excellent agreement between experiments and calculations for the jets with release pressure above 2 bar (deviation 5%) whereas deviation increases to 10% for the release at 2 bar abs. Predictions worsen for the releases with 1 mm diameter nozzle. Reason may be due to the smaller diameter causing an increase of losses and a different heat exchange at the nozzle. Concentration is yet reasonably predicted for the tests characterised by the lowest and highest pressures, respectively 2 and 5 bar abs. Predictions show a deviation for the remaining two tests, arriving up to 25% for release with T=53 K and P=4 bar abs. However, it must be noted that experimental measurements show a more unstable concentration decay along the axis for the 1 mm diameter releases. Two of the experimental tests (including case with T=53 K and P=4 bar abs) present the anomalous behaviour of resulting in a hydrogen concentration along the jet axis lower than tests with lower pressure and higher temperature at the release.

Figure 7 shows that there is a limited effect of the used real gas EOS on the hydrogen concentration decay. Difference in hydrogen concentration is maximum 4.5% at the distance where concentration of ½ LFL is reached (4.5 m) for the release with highest pressure (6 bar abs) and lowest temperature (50 K).

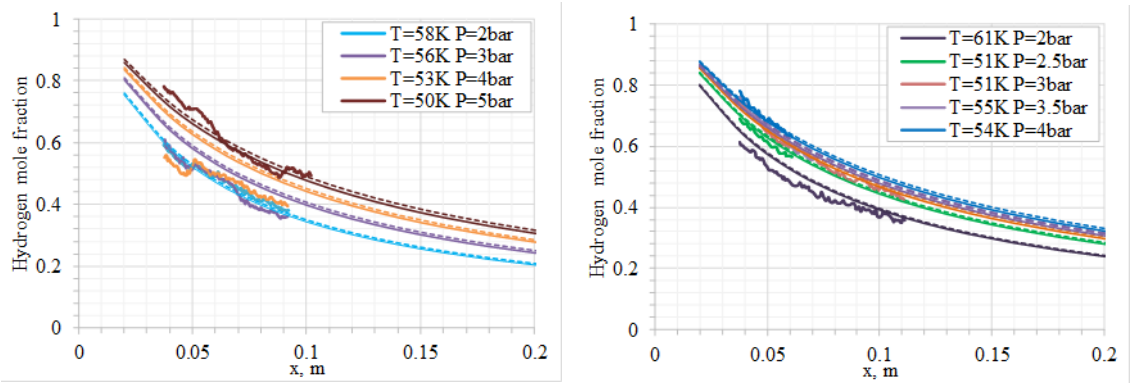

Figure 7. The similarity law estimations using Abel-Noble (dashed lines) and NIST EOSs (thin solid lines) against experiments (thick solid lines) for d=1.00 mm (left) and d=1.25 mm (right)

Figure 8 shows the comparison between SNL experimental data and the similarity law, along with the experimental data reported in Saffers and Molkov (2013) and previously used for validation. Overall, it is showed that the similarity law for axial concentration decay represent well the experiments performed in SNL. Therefore, it can be concluded that the similarity law application can be expanded to temperature down to 50 K for release pressure up to 6 bar abs and be used as an engineering tool to calculate distances to hazardous hydrogen concentration.

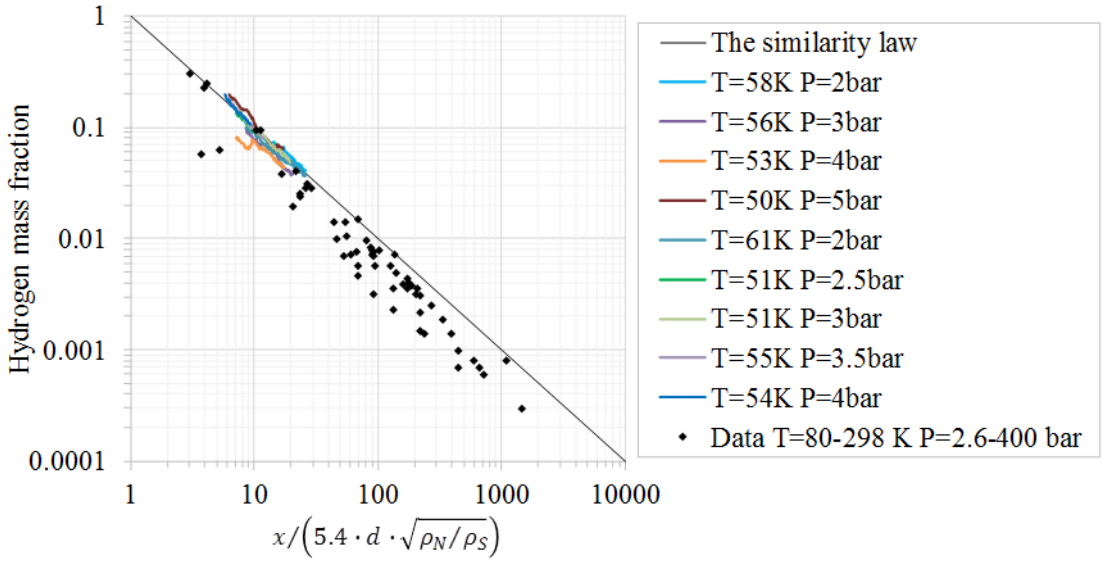

Figure 8. The similarity law and experimental data on axial concentration decay in momentum controlled under-expanded jets from SNL tests and Saffers & Molkov (2013).

6 Conclusions and Future work

A critical review of the modelling work on cryogenic hydrogen release and dispersion has been performed.

The homogeneous mixture approach is currently the dominant CFD mathematical formulation for cryogenic hydrogen flow and dispersion. Most of the simulations work has been performed assuming mechanical and thermal equilibrium. Although mechanical non-equilibrium modelling has been applied in some cases thermal non-equilibrium has not been considered except for 0d release modelling.

Different approaches have been used to treat physical properties of hydrogen and humid air, from pure ideal gas combined with correlations for liquid/solid to most complex equations of state based on Helmholtz free energy for hydrogen.

Different approaches have also been used to treat basic two-phase flow phenomena, such as phase change, slip and rainout, pool vaporization, expansion of cryogenic under-expanded jets, turbulence as well as ground heat transfer.

Future work should focus on performing a systematic inter-comparison of the various proposed approaches based on suitable experiments either from the past or those that are planned within PRESLHY project as well as the Norwegian partner project SH2IFT project.

7 Acknowledgements

The research leading to these results was financially supported by the PRESLHY project, which has received funding from the Fuel Cells and Hydrogen 2 Joint Undertaking under the European Union's Horizon 2020 research and innovation program under grant agreement No 779613.

8 References

Baraldi D., Melideo D., Kotchourko A., Ren K., Yanez J., Jedicke O., Giannissi S.G., Tolias I.C., Venetsanos A.G., Keenan J., Makarov D., Molkov V., Slater S., Verbecke F., Duclos A., Development of a model evaluation protocol for CFD analysis of hydrogen safety issues the SUSANA project, Int. J of Hydrogen Energy, 42 (2017) 7633-7643.

Birch A.D., Brown D.R., Dodson M.G., Swaffield F. (1984), The Structure and Concentration Decay of High Pressure Jets of Natural Gas, Combustion Science and Technology, 36: 5, pp. 249-261.

Birch, A.D., Hughes, D.J., Swaffield, F. (1987), Velocity Decay of High Pressure Jets, Combustion Science and Technology, 52, pp. 161-171.

Brennen C.E., Fundamentals of Multiphase Flows, Cambridge University Press 2005, ISBN 0521 848040.

Britter, R.E., Dispersion of two-phase flashing releases - FLADIS field experiments; the modelling of pseudo-source for complex releases, Report FM89/2 by CERC for EEC Commission DGXII (1994).

Britter, R.E., Dispersion of two-phase flashing releases - FLADIS field experiments; a further note on modelling flashing releases", Report FM89/3 by CERC for EEC Commission DGXII (1995).

Cavanaugh II, T., Siegell, J., & Steinberg, K., Simulation of Vapor Emissions from Liquid Spills, Journal of Hazardous Materials, 38 (1994.) 41–63.

Cheng, N.S., and Law, A.W.K., Exponential formula for computing effective viscosity, Powder Technology. 129 (2003) 156-160

Cirrone, D., Makarov, D. and Molkov, V. (2019a), Cryogenic hydrogen jets: flammable envelope size and hazard distances for jet fire, International Conference on Hydrogen Safety, Adelaide, Australia.

Cirrone, D. M. C., D. Makarov, D. and Molkov, V. (2019b), Thermal Radiation from Cryogenic Hydrogen Jet Fires, International Journal of Hydrogen Energy, vol. 44, no. 17, pp. 8874–8885.

Coldrick S., Lea C.J. and Ivings M .J., Validation Database for Evaluating Vapor Dispersion Models for Safety Analysis of LNG Facilities, Guide to the LNG Model Validation Database, HSL Report Feb. 2009.

Dolci F., Jordan T., Keller J. and Moretto P., Research Priority Workshop on Hydrogen Safety: 26-27 September 2016, Petten, The Netherlands, EUR 29146 EN, Publications Office of the European Union, Luxembourg, 2018, ISBN 978-92-79-80975-0, doi:10.2760/77730, JRC111028

Ekoto I.W., Hecht E., San Marchi C., Groth K.M., LaFleur A.C., Natesan N., and Ciotti M. and Harris A., Liquid Hydrogen Release and Behavior Modeling: State-of-the-Art Knowledge Gaps and Research Needs for Refueling Infrastructure Safety, SANDIA REPORT, SAND2014-18776 Unlimited Release Oct 2014.

Ewan B.C.R., Moodie K., Structure and velocity measurements in under-expanded jets, Combust. Sci. Technol., 45 (1986) 275-288.

Fernandez M.I., Harper M., Mahgerefteh H., and Witlox H.W.M., An integral model for pool spreading, vaporization and dissolution of hydrocarbon mixtures, Symposium Hazards XXIII, 2012 IChem, 466-472

Friedrich A., Breitung W., Stern G., Veser A., Kuznetsov M., Fast G., et al., Ignition and heat radiation of cryogenic hydrogen jets, Int. J. Hydrogen Energy 37 (2012) 17589-17598.

Garcia J., Crespo A., A turbulence model for gas particle jets, Journal of Fluids Engineering, ASME, 122 (2000) 505-509.

GASFLOW-MPI: A Scalable Computational Fluid Dynamics Code for Gases, Aerosols and Combustion, Volume 1: Theory and Computational Model (Revision 1.0), KIT Scientific Report Nr.7710, ISBN 978-3-7315-0448-1, KIT Scientific Publishing, January 2016.

Giannissi S.G., Venetsanos A.G., Markatos N., Bartzis J.G., CFD modeling of hydrogen dispersion under cryogenic release conditions, Int. J. Hydrogen Energy, 39 (2014) 15851-15863.

Giannissi S.G. and Venetsanos A.G., Study of key parameters in modeling liquid hydrogen release and dispersion in open environment, Int. J. of Hydrogen Energy, 43 (2018) 455-467

Giannissi S.G. and Venetsanos A.G., A comparative CFD assessment study of cryogenic hydrogen and LNG dispersion, Int. J. of Hydrogen Energy, 44 (2019) 9018-9030

Giannissi S.G., Venetsanos A.G., Hecht E.S., Numerical Predictions of cryogenic hydrogen vertical jets, 8th Intern. Conf. of Hydrogen Safety, 24-26 Sept. 2019, Adelaide, Australia

Hamzehloo A., Aleiferis P.G., Large eddy simulation of highly turbulent under-expanded hydrogen and methane jets for gaseous-fuelled internal combustion engines, Intern. J. of Hydrogen energy 39 (2014) 21275-21296

Harstad K., Bellan J., Global analysis and parametric dependencies for potential unintended hydrogen-fuel releases, Combust Flame 144 (2006) 89-102

Hecht E.S. and Panda, P. (2016), R&D for Safety, Codes and Standards: Hydrogen Behavior.

Hecht E.S. and Panda P.P., Mixing and Warming of Cryogenic Hydrogen Releases, Int. J. of Hydrogen Energy, (2018) 1–11.

Hooker P., Willoughby D.B., Royle M., Experimental releases of liquid hydrogen, 4th Int. Conf. of Hydrogen Safety (ICHS), September 12-14, 2011, San Francisco, US.

Houf W.G., Winters W.S., Simulation of high-pressure liquid hydrogen releases, Int. J Hydrogen Energy 38 (2013) 8092-8099.

Ichard M., Hansen O.R, Middha P., Willoughby D. CFD computations of liquid hydrogen releases. Int. J. Hydrogen Energy, 37 (2012) 17380-17389.

Jin T., Wu M., Liu Y., Lei G., Chen H., Lan Y., CFD modelling and analysis of the influence factors of liquid hydrogen spills in open environment, Int. J. of Hydrogen Energy, 42 (2017) 732-739.

Khaksarfard R., Kameshki M. R., Paraschivoiu M., Numerical simulation of high pressure release and dispersion of hydrogen into air with real gas model, Shock Waves 20 (2010) 205–216

Kim H-D, Kang M-S, Otobe Y. and Setoguchi T., The effect of non-equilibrium condensation on hysteresis phenomenon of under-expanded jets, Journal of Mechanical Science and Technology 23 (2009) 856~867

Klebanoff L.E., Pratt J.W., LaFleur C.B., Comparison of the safety-related physical and combustion properties of liquid hydrogen and liquid natural gas in the context of the SF-BREEZE high-speed fuel-cell ferry, Int. J. of Hydrogen Energy, 42 (2017) 757-774.

Lagumbay R.S., Vasilyev O.V., Haselbacher A., Homogeneous equilibrium mixture model for simulation of multiphase/multicomponent flows, Int. J. Numer. Methods Fluids, 4 (2007) 1-6.

Leachman J. W., Jacobsen R. T., Penoncello S. G., and Lemmon E. W., Fundamental Equations of State for Parahydrogen, Normal Hydrogen, and Orthohydrogen, J. Phys. Chem. Ref. Data, 38 (2009) 721-748.

Lee W.H., A Pressure Iteration Scheme for Two-Phase Modeling, Technical Report LA-UR, 79-975. Los Alamos, New Mexico: Los Alamos Scientific Laboratory, 1979.

Lemmon E.W., Huber M.L., Mc Linden M.O., NIST standard reference database 23: reference fluid thermodynamic and transport properties-REFPROP, Version 9.1. Gaithersburg, MD: National Institute of Standards and Technology, 2013. Standard reference data program.

Li X. and Christopher D.M., Hecht E.S., Ekoto I.W., Comparison of two-layer model for high pressure hydrogen jets with notional nozzle model predictions and experimental data, 6th Intern. Conf. of Hydrogen Safety, Oct. 19-21, 2015, Yokohama, Japan.

Liao Y., Lucas D., Computational modelling of flash boiling flows: A literature survey, International Journal of Heat and Mass Transfer 111 (2017) 246–265.

Liu Y., Wei J., Lei G., Lan Y., Chen H., Jin T., Dilution of hazardous vapor cloud in liquid hydrogen spill process under different source conditions. Int. J. Hydrogen Energy 43 (2018) 7643–7651

Lyras K., Dembele S., Schmidt D.P., Wen J.X., Numerical simulation of subcooled and superheated jets under thermodynamic non-equilibrium, International Journal of Multiphase Flow, 102 (2018) 16-28

Manninen M., Taivassalo V., Kallio S.. On the mixture model for multiphase flow. Technical Research Center of Finland, VTT Publications; 1996. p. 288.

Marinescu-Pasoi L, Sturm B., Messung der Ausbreitung einer Wasserstoff und Propangaswolke in bebautem Gelände and Gasspezifische Ausbreitungsversuche, Battelle Ingenieurtechnik GmbH Reports R-68.202 and R-68.264; 1994.

Markert F., Melideo D., Baraldi D., Numerical analysis of accidental hydrogen releases from high pressure storage at low temperatures, Int. J. of Hydrogen Energy, 39 (2014) 7356-7364.

Mathias P.M., Copeman T.W., Extension of the Peng-Robinson equation-of-state to complex mixtures: evaluation of the various forms of the local composition concept. Fluid Phase Equilib. 13 (1983) 91-108.

Mauri L. Private communication (2019)

Michelsen M.L., Calculation of multiphase equilibrium, Computers Chem. Engng. 18 (1994) 545-550.

Middha P., Ichard M., Arntzen B., Validation of CFD modelling of LH2 spread and evaporation against large-scale spill experiments, International Journal of Hydrogen Energy, 36 (2011) 2620-2627.

Molkov V., Makarov D., Prost E., On numerical simulation of liquefied and gaseous hydrogen releases at large scales, 1rst International Conference on Hydrogen Safety, 8-10 September 2005, Pisa, Italy.

Molkov, V., Makarov, D. and Bragin, M. V. (2009), Physics and Modelling of Underexpanded Jets and Hydrogen Dispersion in Atmosphere, Physics of Extreme States of Matter, pp. 146–149.

Molkov, V. (2012), Fundamentals of Hydrogen Safety Engineering I, Free-download electronic book available at www.bookboon.com. Download free books at bookboon.com.

Nasrifar K., Comparative study of eleven equations of state in predicting the thermodynamic properties of hydrogen, Int. J. of Hydrogen Energy, 35 (2010) 3802-3811.

NIST, NIST EoS Calculator [Online], Available: https://h2tools.org/hyarc/calculator-tools/equation-state-calculator. [Accessed: 26-Mar-2019].

Panda P.P. and Hecht E.S., Ignition and Flame Characteristics of Cryogenic Hydrogen Releases, Int. J. of Hydrogen Energy, 42 (2017) 775–785.

Papanikolaou E., Baraldi D., Kuznetsov M., Venetsanos A., Evaluation of notional nozzle approaches for CFD simulations of free-shear under-expanded hydrogen jets, Int. J. of Hydrogen Energy, vol. 37 (2012) 18563-18574.

Poling B.E., Prausnitz J.M., O'Connell J.P., The Properties of Gases and Liquids, Fifth Edition, McGraw-Hill, 2004

Proust C., Chelhaoui S., Joly C., Processes of the formation and explosion of hydrogen-air clouds following an extensive spillage of liquid hydrogen, National Hydrogen Association 12th Annual U.S. Hydrogen Meeting and Exposition, 2001

Saffers, J. B. and Molkov, V. V. (2013), Towards Hydrogen Safety Engineering for Reacting and non-Reacting Hydrogen Releases, Journal of Loss Prevention in the Process Industries, vol. 26, no. 2, pp. 344–350.

Schefer, R.W., Houf, W.G., Williams, T.C., Bourne, B., Colton J., Characterization of high-pressure, underexpanded hydrogen-jet flames, Int. J. of Hydrogen Energy 32 (2007) 2081-2093

Shevyakov, G.G., Tomilin, V.P., Kondrashkov, Y.A. (1980), Engineering Physical Journal, deposit with VINITI, N3671-80 (in Russian).

Simoneau R. and Hendricks R., Two-phase choked flow of cryogenic fluids in converging-diverging nozzles, NASA Tech. Rep. Pap. 1484, 1979.

Sklavounos S. and Rigas F., Fuel Gas Dispersion under Cryogenic Release Conditions, Energy & Fuels 19 (2005) 2535-2544

Statharas, J.C., Venetsanos, A.G., Bartzis, J.G., Würtz, J., Schmidtchen, U., Analysis of data from spilling experiments performed with liquid hydrogen, J. Hazardous Materials A77 (2000) 57-75

TNO Yellow Book (1979).

Tolias I.C., Giannissi S.G., Venetsanos A.G., Keenan J., Shentsov V., Makarov D., Coldrick S., Kotchourko A., Ren K., Jedicke O., Melideo D., Baraldi D., Slater S., Duclos A., Verbecke F., Molkov V., Best practice in numerical simulation and CFD benchmarking. Results from the SUSANA project, 7th International Conference on Hydrogen Safety (ICHS 2017), Hamburg, Germany, 11-13 September, 2017.

Travis J.R., Piccioni Koch D., Breitung W., A homogeneous non-equilibrium two-phase critical flow model, Int. J. Hydrogen Energy, 37 (2012) 17373-17379.

Travis J.R., Piccioni Koch D., Xiao J., Xuc Z., Real-gas Equations-of-State for the GASFLOW CFD code, Int. J. Hydrogen Energy, 38 (2013) 8132-8140.

Venetsanos A.G., Bartzis J.G., CFD modelling of large-scale LH2 spills in open environment, Int. J. Hydrogen Energy, 32 (2007), 2171-2177.

Venetsanos A.G. and Giannissi S.G., Release and dispersion modelling of cryogenic under-expanded hydrogen jets, Int. J of Hydrogen Energy, 42 (2017) 7672-7682

Venetsanos A.G., Homogeneous non-equilibrium two-phase choked flow modelling, Int. J. of Hydrogen Energy, 43 (50), 22715-22726 (2018)

Venetsanos A.G., Giannissi S., Proust C., CFD validation against large scale liquefied helium release, Intern. Conf. Hydrogen Safety (ICHS-8), 24-26 Sept. 2019, Adelaide, Australia.

Venetsanos A.G., Choked two-phase flow with account of discharge line effects, 8th Intern. Conf. on Hydrogen Safety, 24-26 Sept. 2019, Adelaide, Australia

Verfondern K, Safety considerations on liquid hydrogen, Energy and Environment, Vol. 10, Forschungszentrum Julich 2008, ISBN 978-3-89336-530-2, 178 pages.

Verfondern K, Dienhart B. Experimental and theoretical investigation of liquid hydrogen pool spreading and vaporization. Int J Hydrogen Energy, 22 (1997) 649–660.

Veser A., Kuznetsov M., Fast G., Friedrich A., Kotchourko N., Stern G,. et al., The structure and flame propagation regimes in turbulent hydrogen jets, Int. J. Hydrogen Energy 36 (2011) 2351-2359.

Walas, S. M., 1985. Phase equilibria in chemical engineering. London.

Webber D.M., Gant S.E., Ivings M.J. and Jagger S.F., LNG Source Term Models for Hazard Analysis: a Review of the State-of-the-Art and an Approach to Model Assessment, HSL Report Feb. 2009.

Witlox H.W.M., Bowen P.J., Flashing liquid jets and two-phase dispersion: A review, HSE Books, ISBN 0 7176 2250 9, 2002,

Witcofski R.D., Chirivella J.E., Experimental and analytical analyses of the mechanisms governing the dispersion of flammable clouds formed by liquid hydrogen spills, Int. J Hydrogen Energy 9 (1984) 425–435.

Xiao J., Travis J.R., Breitung W., Hydrogen release from a high pressure gaseous hydrogen reservoir in case of a small leak, Int. J Hydrogen Energy 36 (2011) 2545–2554.

Yuceil K.B., Otugen M.V., Scaling parameters for under-expanded supersonic jets. Phys. Fluids 14 (2002) 4206-4215